Electronic transport properties of single-crystal bismuth nanowire arrays

Zhibo Zhang* and Xiangzhong Sun†
Department of Physics, Massachusetts Institute of Technology, Cambridge, Masscahusetts 02139-4307

M. S. Dresselhaus‡
Department of Physics and Department of Electrical Engineering and Computer Science, Massachusetts Institute of Technology, Cambridge, Massachusetts 02139-4307

Jackie Y. Ying
Department of Chemical Engineering, Massachusetts Institute of Technology, Cambridge, Massachusetts 02139-4307

J. Heremans
Delphi Automotive Systems, Central Research & Development, Warren, Michigan 48090-9055
(Received 17 May 1999; revised manuscript received 18 August 1999)

We present here a detailed study of the electrical transport properties of single-crystal bismuth nanowire arrays embedded in a dielectric matrix. Measurements of the resistance of Bi nanowire arrays with different wire diameters (60–110 nm) have been carried out over a wide range of temperatures (2.0–300 K) and magnetic fields (0–5.4 T). The transport properties of a heavily Te-doped Bi nanowire array have also been studied. At low temperatures, we show that the wire boundary scattering is the dominant scattering process for carriers in the undoped single-crystal Bi nanowires, while boundary scattering is less important for a heavily Te-doped sample, consistent with general theoretical considerations. The temperature dependences of the zero-field resistivity and of the longitudinal magneto-coefficient of the Bi nanowires were also studied and were found to be sensitive to the wire diameter. The quantum confinement of carriers is believed to play an important role in determining the overall temperature dependence of the zero-field resistivity. Theoretical considerations of the quantum confinement effects on the electronic band structure and on the transport properties of Bi nanowires are discussed. Despite the evidence for localization effects and diffusive electron interactions at low temperatures ($T \leq 4.0$ K), localization effects are not the dominant mechanisms affecting the resistivity or the magnetoresistance in the temperature range of this study.

I. INTRODUCTION

The electrical transport properties of ultrafine metal and semiconductor wires have been a subject of growing interest. Early studies were focused on classical size effects, for which detailed theories have been established,[1,2] and some theoretical predictions have been confirmed by experimental results for bismuth wires.[3] More recently, localization effects,[4] which are quantum interference effects, in disordered systems with reduced dimensionalities have also been studied in general and in Bi nanowires in particular.[5,6] In the past decade, impressive progress has been made in experimental studies of electron transport in quantum nanocontacts formed in GaAs/AlAs heterostructures[7] or generated by using the mechanically controllable break junction technique[8] or by using a scanning tunneling microscope operating in the contact mode.[9] The nanocontacts in these experiments have been shown to be in the ballistic regime so that the transverse momentum of electrons becomes discrete. Since the nanocontacts are short in length, the phenomena observed in these systems, such as conductance quantization in units of $2e^2/h$, are found to be materials independent.[10] In sophisticated quantum wire systems, which generally have a large aspect ratio (length/diameter), the two-dimensional quantum confinement of the resulting quasi-one-dimensional (1D) electron gas provides a method to manipulate the electronic transport properties of materials by changing their electronic density of states. This gives rise to a wide range of opportunities for utilizing the electronic transport properties of various quasi-1D materials systems for various practical device applications.

Recently, we have successfully fabricated Bi nanowire arrays by pressure injection of liquid-Bi melt into the nanochannels of an anodic alumina template.[11] Bi nanowires are of special interest for thermoelectric applications[12] due to the unique properties of bulk Bi, such as its small electron effective mass components, the high anisotropy of its Fermi surface and the low thermal conductivity of Bi. Experimental thermopower values for 200-nm-diameter wires prepared using alumina templates have been reported.[13] Also because of the small Bi electron effective mass components, Bi nanowires provide an excellent system to study the effect of quantum confinement on the electronic transport properties of quasi-1D systems. Since the Bi nanowires that we produced are single crystals, the scattering processes for carriers are also expected to be different from those in polycrystalline Bi thin wire systems that have previously been studied.[5] Since the Bi nanowires also have a very large aspect ratio, the electrons may experience numerous collisions with the wire boundary during their conduction. Studying the transport properties of Bi nanowires could also provide an opportunity to verify the theories[1,2] established in early studies of the electrical conductivity of thin wires, but are now studied in a smaller wire diameter regime.

0163-1829/2000/61(7)/4850(12)/$15.00 ©2000 The American Physical Society

In this paper, we present a detailed study of the electronic transport properties of this interesting class of nanostructured materials. Specifically, we have measured the resistance of Bi nanowire arrays with various wire diameters (60–110 nm) over a wide range of temperatures (2.0–300 K) and magnetic fields (0–5.4 T). The transport properties of a 0.1 at. % Te-doped Bi nanowire array have also been studied. In Sec. II, we briefly describe the sample fabrication and characterization processes and also the experimental procedures for the transport measurements. In Sec. III, we present a theoretical model for the electron subband structure of the quasi-1D Bi nanowires, based on the basic band structure of bulk Bi. Section IV presents the experimental results and discussion. First, we found that the temperature dependence of the zero-field resistivity is very sensitive to the wire diameter, showing evidence for a transition from metallic behavior to semiconducting behavior when the wire diameter is reduced.[14] The experimental results are consistent with the electronic subband structure of Bi nanowires that we construct in Sec. III. In the magnetoresistance (MR) studies, we found that the behaviors of the longitudinal magnetoresistance and the transverse magnetoresistance of pure Bi nanowire arrays are very different from each other, and that they are also different from the behavior of the Te-doped Bi nanowire sample. These differences are explained by the dominant wire boundary scattering process for carriers in pure single-crystal Bi nanowires at low temperatures, in contrast to the theoretical expectation for an ideal quantum wire system. We also found that the temperature dependence of the longitudinal magnetocoefficient is very sensitive to the wire diameter. In the last part of Sec. IV, we provide experimental evidence for localization effects and diffusive electron-electron interactions, which are important only at very low temperatures ($T \leqslant 4.0$ K). The experimental results for diffusive electron conduction observed in our single-crystal Bi nanowires are consistent with those of polycrystalline Bi nanowires.[5] Finally, in Sec. V, we present our conclusions.

II. SAMPLE PREPARATION AND EXPERIMENTAL PROCEDURES

The Bi nanowire arrays were fabricated by a template-assisted approach described elsewhere.[11,15] The anodic alumina templates, having an array of parallel nearly cylindrical channels, are produced by anodizing aluminum substrates in acid solutions. Using a vacuum melting and pressure injection process, liquid Bi is forced into the evacuated channels of the anodic alumina template at a temperature higher than the melting point of Bi (~271.5 °C). Copper impurities, which have a small solubility in liquid Bi (~0.2 at.% at 325 °C) and essentially no solubility in a solid Bi crystal, were used to improve the Bi filling of the channels in the anodic alumina templates. By slowly cooling the system down to room temperature, an array of essentially single-crystal Bi nanowires was produced. Since the anodic alumina templates are fragile, the templates were broken into small pieces during the sample preparation,[11,15] and therefore the areas of the samples used in the measurements were about 2–5 mm^2, although the initial areas of the anodic alumina templates used in our experiments were larger than 1 cm^2. For some measurements, the samples were then annealed for 8 h at 150 °C under flowing N_2. Because Bi may form a thin oxide layer on the surface upon exposure to air, we always stored the samples inside a glove box in which Ar gas was circulated.

TABLE I. Characteristics of the Bi nanowire arrays investigated in the electrical transport studies. All samples have the primary crystal orientation along the wire axis perpendicular to the (202) lattice plane.

Sample no.	Wire dia. (nm)	Cell size (nm)	Wire length (μm)	Composition
A	65±8	~125	~45	pure Bi
B	90±14	~150	~65	pure Bi
C	109±24	~165	~50	pure Bi
D	60±8	~125	~40	$Bi_{0.999}Te_{0.001}$

For this study, we prepared three undoped Bi nanowire arrays with wire diameters of 65±8, 90±14, and 109±24 nm, and a 0.1 at. % Te-doped Bi nanowire array with a wire diameter of 60 ± 8 nm and the characteristics of these samples are given in Table I. The average distances between the centers of adjacent wires varied from 125 to 165 nm and the template thicknesses (or wire lengths) of the samples were 40–65 μm, with a variation in wire diameter for individual nanowires along their wire lengths of ±10%. We used high-purity Bi (99.999%) pieces and a $Bi_{0.999}Te_{0.001}$ alloy as starting materials to produce pure Bi nanowires and 0.1 at. % Te-doped Bi nanowires, respectively.

The materials properties of the fabricated Bi nanowire arrays were investigated by various characterization techniques, such as x-ray diffraction (XRD), scanning electron microscopy (SEM), transmission electron microscopy (TEM), and selected area electron diffraction (SAED).[11,15] The single crystallinity and orientation of the Bi nanowires were confirmed by both high-resolution electron microscopy (HREM) and SAED studies on free-standing Bi nanowires, which were prepared by dissolving away the anodic alumina template in a special acid solution. XRD experiments revealed that all the wires in a nanowire array are highly oriented along the wire axis, with more than 90% of the wires being oriented along a crystal direction normal to the (202) lattice plane of the rhombohedral crystal structure of Bi.[14,15] In the XRD experiments, we found that all the strong diffraction peaks are close to the peak positions of a polycrystalline Bi standard, revealing that the rhombohedral crystal structure of bulk Bi is also preserved in the small diameter Bi nanowires.[11,14]

Due to the limitations imposed by the sample geometry [see inset in Fig. 2(a)], we used a two-probe dc technique in the electronic transport measurements by bringing Au wire electrodes to both sides of the Bi nanowire composite using conducting silver paint contacts about 1–2 mm^2 in size. Since the silver particle size in the silver paint is on the order of 1 μm, the silver paint may only make good contact to a small fraction of the total number of wires of the sample. For this reason, we could not estimate the total number of wires connected to the two contacts, and the actual resistivity of the nanowires is therefore unknown. The resistance of the various samples was between several ohms to several thousand ohms, and the absolute value of the zero-field resistance

(adjusted by the area) was normally different between different pieces of the nanowire array obtained from the same sample. However, when we normalized the zero-field resistance to the value at a common temperature (i.e., 300 K), and normalized the magnetoresistance to the zero-field resistance, the T dependences of the normalized zero-field resistance and the normalized magnetoresistance became very repeatable. The zero-field resistance and the magnetoresistance measurements were made within the chamber of a superconducting quantum interference device magnetometer operating in the temperature range of 2.0–300 K and in the magnetic field range of 0–5.4 T. Before each measurement, the sample was taken out from the glove box and was exposed to air, sometimes for several hours. However, we found that sample degradation was not a big concern, and the repeatability of the measurements between different runs for the same piece of the sample was excellent.

III. ELECTRONIC BAND STRUCTURE OF Bi QUANTUM WIRES

Since the diameter d of the Bi nanowires studied in this work is much smaller than the mean free path l_e of electrons in Bi, especially at low temperatures, the electrons will experience quantum confinement effects, which is one of the most important factors in determining the electrical transport properties of Bi nanowires. This confinement not only directly affects the carrier concentration in Bi nanowires, but will also influence more delicate issues, such as the wire boundary scattering of the carriers and the magnetoresistance tensor for Bi nanowires.

Bi is a semimetal with a rhombohedral ($R\bar{3}m$) crystal structure[16] and a small band overlap [$E_g = -38$ meV (Ref. 17)] between the fifth band and the sixth band.[18] The Fermi surface of bulk Bi in the Brillouin zone consists of a single hole pocket at the T point and three highly elongated electron pockets at the L point. The hole pocket is described by a simple effective mass tensor with $m_{h1} = m_{h2} = 0.059m_0$, $m_{h3} = 0.634m_0$, where m_0 is the free electron mass.[17] The electron effective mass tensors are complicated by the small tilt angle θ of the long axis of the electron ellipsoids from the bisectrix axis towards the trigonal direction, with the effective mass tensor for the electron pocket along the bisectrix axis (denoted by A) given by

$$\mathbf{M_e} = \begin{pmatrix} m_{e1} & 0 & 0 \\ 0 & m_{e2} & m_{e4} \\ 0 & m_{e4} & m_{e3} \end{pmatrix}, \tag{1}$$

where $m_{e1} = 0.00139m_0$, $m_{e2} = 0.291m_0$, $m_{e3} = 0.0071m_0$, $m_{e4} = -0.0359m_0$ at the band edge.[17,19] The effective mass tensors for the other two electron pockets (denoted by B and C) are obtained by rotating Eq. (1) about the trigonal axis by $\pm\frac{2}{3}\pi$. The dispersion relations are approximately parabolic for holes below the band edge, but are strongly nonparabolic for electrons[18] due to the small L-point band gap [$E_{gL} = 15$ meV (Ref. 17)] and the small electron effective mass components. The Lax model,[20] which was derived from a two-band model using Brillouin-Wigner perturbation theory to describe the strongly coupled conduction and valence bands at the L points, gives the 3D electron energy states as

$$E(\mathbf{k}) = \sqrt{\frac{E_{gL}^2}{4} + E_{gL}\frac{\hbar^2}{2}\mathbf{k}\cdot\mathbf{M_e}^{-1}\cdot\mathbf{k}} - \frac{E_{gL}}{2}, \tag{2}$$

where E is measured with respect to the energy of the L-point conduction-band edge, and $\mathbf{M_e}$ is the electron effective mass tensor at the band edge.

When electrons are confined inside a nanowire, the allowed transverse momenta for electrons become discrete, and the electronic energy states are split into subbands. Since Bi has very small electron effective mass components, the formation of subbands becomes important for Bi nanowires with diameters on the order of 100 nm, much larger than is common for other materials. Following the Lax model [Eq. (2)] and using a cylindrical potential-well approximation, the dispersion relations for the nonparabolic electron pockets in a Bi quantum wire can be expressed as

$$E_{ij}(k_l) \approx \sqrt{\frac{E_{gL}^2}{4} + E_{gL}\left(\frac{\hbar^2 k_l^2}{2m_l^*} + \frac{2\hbar^2\chi_{ij}^2}{m_c^* d_w^2}\right)} - \frac{E_{gL}}{2}, \tag{3}$$

where χ_{ij} are roots of the Bessel function $J_i(\chi_{ij}) = 0$, d_w is the wire diameter, m_c^* is the cyclotron effective mass in the transverse plane, and k_l and m_l^* are, respectively, the electron momentum and the effective mass component along the wire axis. Both m_c^* and m_l^* are electron effective mass components at the band edge of bulk Bi. Since the Bi nanowires studied in this work have a well-defined crystal orientation along the wire axis, while the crystal orientation in the transverse plane is very likely to be random for the various nanowires in a nanowire array, it is appropriate to use an average mass for the effective mass components in the transverse plane where quantum confinement occurs. This average is conveniently approximated by the cyclotron effective mass m_c^*. In Eq. (3) the subband onsets are treated within the Lax model, while the dispersion along the wire direction is treated in terms of a parabolic k_l dependence based on perturbation theory.

As shown in the XRD data, the majority of the Bi nanowires in each array were oriented along a crystal direction perpendicular to the (202) lattice plane. The direction perpendicular to the (202) lattice plane in real space is $[10\bar{1}1]$ (using the space group $R\bar{3}m$ and the hexagonal structural description[16]) in k space, which corresponds to

$$\hat{l} = (0,0.949,0.315) \tag{4}$$

in the Cartesian coordinate system where x, y, z represent the binary, bisectrix, and trigonal directions, respectively.

Following Eq. (3), we calculate the electronic subband structure for Bi nanowires of different wire diameters using the values of the effective masses given in Ref. 17. The results for the electronic subband structures of $[10\bar{1}1]$ wires are shown in Fig. 1, treating the L-point electron and hole bands as mirror bands, following the two-band Lax model. For the $[10\bar{1}1]$ crystal orientation, the electron pocket A has a very small cyclotron effective mass ($m_c^* = 0.002\,12m_0$), while the other two electron pockets (B and C) are equivalent and have a cyclotron effective mass ($m_c^* = 0.003\,72m_0$) about two times heavier than that of electron pocket A. Thus the energy of the lowest subband edge of

electron pocket A increases faster with decreasing wire diameter d_w than for the lowest subband edge of electron pockets B and C, thus resulting in the splitting of the L-point band edge, as shown in Fig. 1. Since m_l^* for electron pockets B and C ($m_l^*=0.0779m_0$) is smaller than for electron pocket A ($m_l^*=0.241m_0$), the band curvature for the dispersion relation $E_{ij}(k_l)$ is greater for carrier pockets B and C than for A, as shown in Fig. 1. In this figure we see that as the wire diameter d_w decreases, E_{gL} increases, while the band overlap energy decreases. Bi nanowires thus are expected to undergo a semimetal-to-semiconductor transition when the wire diameter is reduced below a critical value d_c, as discussed below.

The effective band-gap energy E_g' between the lowest L-point electron subband and the highest T-point hole subband is given by

$$E_g'=\frac{2\hbar^2\chi_{10}^2}{m_{ch}^*d_w^2}+\sqrt{\frac{E_{gL}^2}{4}+E_{gL}\frac{2\hbar^2\chi_{10}^2}{m_{ce}^*d_w^2}}-\frac{E_{gL}}{2}+E_g. \quad (5)$$

We note that in the limit of large d_w, then $E_g'\rightarrow E_g$. The first term in Eq. (5) reflects the parabolic approximation used to describe the highest T-point hole subband where m_{ch}^* is the cyclotron effective mass of holes. Since Fig. 1 shows that the lowest L-point conduction subband only involves the B and C electron carrier pockets, with the subband A lying higher in energy, m_{ce}^* is the cyclotron effective mass of electrons in carrier pockets B and C at the 3D band edge. Using Eq. (5), we can calculate the effective band-gap energy E_g' as a function of wire diameter d_w for Bi nanowires with any crystal orientations. If we define d_c as the diameter at which the Bi nanowires undergo a semimetal-to-semiconductor transition ($E_g'=0$), then $d_c=45$, 44, 33, and 20 nm for Bi nanowires oriented along the $[10\bar{1}1]$, bisectrix, trigonal, and binary directions, respectively. These values for d_c are smaller than those obtained when nonparabolic effects of the L-point conduction band are ignored.[14]

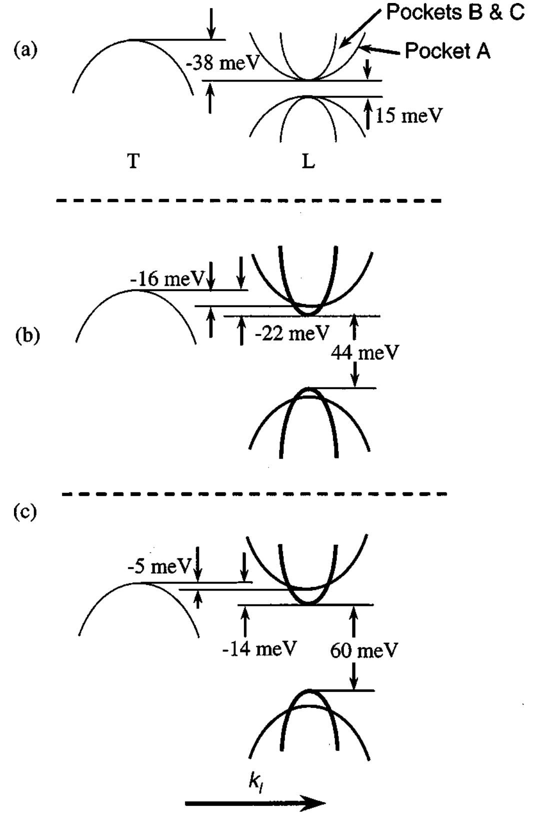

FIG. 1. Schematic energy-band diagram showing the energies of the lowest subband edges for the three L-point electron pockets (A, B, and C) and the highest subband edge for the T-point and L-point holes for: (a) bulk Bi, where the L-point bulk band gap is 15 meV, (b) 90-nm-diameter Bi nanowires, and (c) 65-nm-diameter Bi nanowires, both oriented along the $[10\bar{1}1]$ direction. The energy dispersion relation for each subband shown is for the wave vector along the wire axis k_l, while the band-edge energy of each subband is determined by the average in-plane effective mass, approximated here by the appropriate effective cyclotron mass.

IV. EXPERIMENTAL RESULTS AND DISCUSSION

A. Temperature dependence of zero-field resistivity

We first measured the T dependence of the zero-field resistance $R(T)$ of Bi nanowire arrays. According to the theory discussed in Sec. III, we expected that $R(T)$ should show a transition from metallic behavior to semiconducting behavior as the wire diameter is reduced. However, $R(T)$ is complicated in Bi nanowires because both the carrier mobility and the carrier concentration have a strong T dependence.[21,22] Figure 2(a) shows the results for $R(T)$ for Bi nanowire arrays of two different wire diameters in comparison with the literature data for single-crystal bulk Bi.[23,24] The nanowire arrays were thermally annealed at 150 °C for 8 h under flowing N_2 before the measurements. Since the total number of wires connected between the electrical contacts was unknown for each sample, the absolute value of the measured resistance cannot be related to that of a single nanowire. Therefore the data presented in Fig. 2(a) were normalized to the resistance at $T=300$ K, and the resulting $R(T)/R(300\text{ K})$ can be interpreted as a normalized temperature-dependent resistivity.

Bulk Bi is a semimetal with a narrow-band overlap, and its carrier concentration increases significantly with increasing T above ~70 K (electron concentration $n_e=2.73\times10^{17}$ cm^{-3} and 2.45×10^{18} cm^{-3} at $T=4.2$ and 300 K, respectively.[24,25]) The increasing carrier concentration and decreasing carrier mobility in bulk Bi happen to yield a zero-field resistivity that has a nearly linear dependence on T above ~70 K. For Bi nanowires, we note that the observed T dependence of their resistivity (Fig. 2) is very different from that of bulk Bi and is very sensitive to the wire diameter. At high temperatures ($T>70$ K), the resistivity of both nanowire arrays (90 and 65 nm diameters) decreases with increasing T, while at low temperatures, the T dependences are very different for the two arrays with different wire diameters. When $T<70$ K, the resistivity of the 65-nm sample continues to increase with decreasing temperature, while the resistivity decreases with decreasing temperature for the 90-nm sample. The general trend observed in Fig. 2(a) is consistent with the previous results on single-crystal Bi thin wires of larger diameters $d_w\geqslant200$ nm.[3,6,26,27]

In order to explain the experimental results of $R(T)$ shown in Fig. 2(a), we need to take the quantum confinement effect into account. Based on the calculated subband struc-

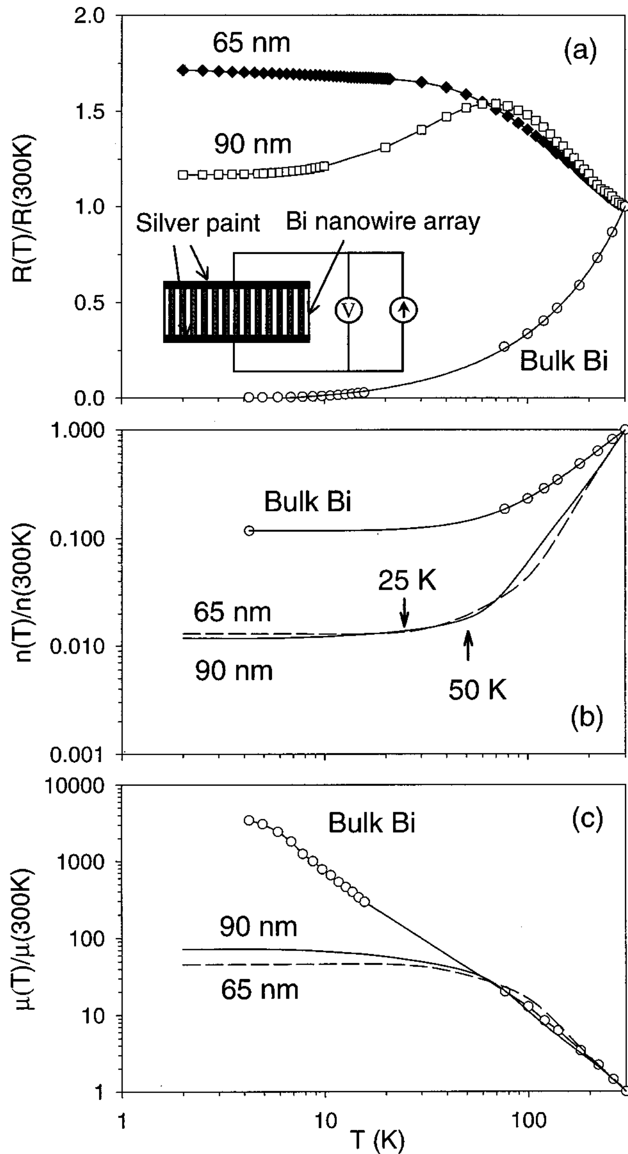

FIG. 2. (a) T dependence of the resistance for Bi nanowire arrays with average diameters of 65 and 90 nm after thermal annealing at 150 °C for 8 h. The data for bulk Bi are obtained from Refs. 23 and 24. The inset shows a schematic diagram of the two-probe dc technique used for the measurements of electrical transport properties of Bi nanowire arrays. (b) Calculated normalized carrier concentration as a function of T for Bi nanowires with wire diameters of 65 and 90 nm. The calculations are based on the electronic band structure of Bi nanowires shown in Fig. 1. The data for bulk Bi are obtained from Refs. 24 and 25. (c) Calculated normalized average electron mobility as a function of T for Bi nanowire arrays with wire diameters of 65 and 90 nm, in comparison with bulk Bi (Refs. 23 and 24). The calculations are based on the measured T dependence of the resistance shown in (a) and the calculated T dependence of the carrier concentration shown in (b).

tures (see Fig. 1, where only the lowest subband for each electron and hold pocket is shown), we calculated the T dependence of the carrier concentration (normalized to 300 K) for Bi nanowires of both wire diameters, and the calculated results are shown in Fig. 2(b) on a log-log scale. In our model calculation, we included the first four subbands for each electron and hole pocket, and higher subbands are approximated by the continuous 3D density of states. For simplicity, the T dependence of the band parameters of bulk Bi[21,22] is neglected in the present work. Although the absolute values of the calculated carrier concentrations are quite different for Bi nanowires with diameters of 65 and 90 nm, when normalized to 300 K, their T dependences are quite similar. At low temperatures ($T<T_0$, where T_0 is wire diameter dependent, and $T_0\approx 25$ and 50 K for $d_w=65$ and 90 nm, respectively), the carrier concentrations of both wires show a very small temperature dependence, similar to that of bulk Bi at $T<T_0\approx 70$ K. For $T>T_0$, the carrier concentrations of both nanowires increase dramatically with increasing T, increasing faster than for bulk Bi. A decreasing T_0 with decreasing d_w can be explained by the decrease in the band overlap E'_g with decreasing d_w. For a conventional metal with a large overlap between the valence and conduction bands (normally on the order of eV), the T dependence of the carrier density can only be observed at very high temperatures. While Bi is a semimetal with a narrow-band overlap ($E_g=-38$ meV), the thermal excitation of carriers from the valence band to the conduction band becomes important when $T\gtrsim 70$ K. Since the band overlap E'_g in Bi nanowires is further reduced, the thermal excitation of carriers from the T-point valence band to the L-point conduction band can be observed at an even lower temperature. Consequently T_0 decreases with decreasing d_w.

Since bulk Bi is a semimetal, both electrons and holes contribute to its electrical conductivity (σ). Similarly in a Bi quantum wire, σ can be expressed as a sum of contributions from each electron and hole subband. For simplicity, we neglect the E dependence of the effective mass tensor for a given subband and include the nonparabolic effects regarding each subband edge. Then, the T dependence of the zero-field conductivity of a Bi quantum wire can be expressed as

$$\sigma(T)=\sum_i \frac{n^{(i)}(T)e^2\tau(T)}{\mathbf{M}^{(i)}}, \tag{6}$$

where $\tau(T)$ is the temperature-dependent relaxation time and $\mathbf{M}^{(i)}$ is either the effective mass tensor of holes (all hole subbands have the same effective mass tensor) or the effective mass tensor of electrons at the edge of the ith electron subband in accordance with the approximations stated above. For each electron subband, $\mathbf{M}^{(i)}$ can be calculated from Eq. (2), and

$$\mathbf{M}^{(i)}\approx\frac{2E^{(i)}+E_{gL}}{E_{gL}}\mathbf{M}_e, \tag{7}$$

where $E^{(i)}$ is the onset energy of the ith electron subband measured from the 3D band edge of the L-point electron pockets, and $\mathbf{M}_e$ is the effective mass tensor of electrons at the 3D band edge. A similar equation also holds for L-point holes.

Based on the T dependence of the carrier concentration presented in Fig. 2(b) and the measured $R(T)$ shown in Fig. 2(a), we can determine the T dependence of the carrier mobility $[\mu(T)=\sigma(T)/n(T)e]$ of Bi nanowires following Eq. (6). The carrier mobilities as a function of T thus determined are shown in Fig. 2(c) for both nanowire samples. For these

two Bi nanowire arrays, the normalized $\mu(T)$ is comparable to that of bulk Bi for $T>70\,\mathrm{K}$. However, the temperature dependence of $\mu(T)$ is much weaker (by more than one order of magnitude) for nanowires compared to that for bulk Bi for $T<70\,\mathrm{K}$. At high temperatures [the Debye temperature of bulk Bi is about 100 K (Refs. 28 and 29)], phonon scattering is the most important scattering process for carriers in Bi nanowires, so that in this temperature range, the T dependence of the carrier mobility in Bi nanowires is expected to be quite similar to that of bulk Bi. The large increase in the carrier concentration with increasing T for $T>70\,\mathrm{K}$ (see discussion above) outweighs the decrease of carrier mobility for both nanowire samples, and therefore their resistivities decrease with increasing T over this temperature range. However at low temperatures, the dominant scattering mechanism for carriers is wire boundary scattering (see detailed discussion in Sec. IV B), making the carrier mean free path and carrier mobility relatively insensitive to T. We can see from Fig. 2(c) that for $T<70\,\mathrm{K}$, the carrier mobility of the 90-nm sample increases faster with decreasing temperature than that of the 65-nm sample, consistent with the fact that the wire boundary scattering for carriers is stronger in a smaller wire. For the 90-nm sample at $T<T_0\approx 50\,\mathrm{K}$, the increase in carrier mobility with decreasing T can therefore outweigh the small decrease in carrier concentration, so that the total resistivity decreases with decreasing T [see Fig. 2(a)]. However, for the 65-nm sample at $T<T_0\approx 25\,\mathrm{K}$, the T dependence of the carrier mobility not only is very small, but Fig. 2(c) actually indicates a slightly decreasing carrier mobility with decreasing T at $T<10\,\mathrm{K}$. Consequently, the overall resistivity of the 65-nm sample continues to increase with decreasing T at low temperatures. A decrease in μ with decreasing T at $T<10\,\mathrm{K}$ for the 65-nm sample may be attributed to the diffusive electron-electron interaction, which will be discussed in more detail in Sec. IV D.

To study the effect of thermal annealing on $R(T)$, we also measured $R(T)$ for the as-prepared Bi nanowire arrays before thermal annealing, and the results are shown in Fig. 3(a). It is surprising to see that $R(T)/R(300\text{ K})$ is not sensitive to the wire diameter before thermal annealing. A possible reason for this is the higher impurity and defect levels in the as-prepared samples, so that both the carrier concentration and the carrier mobility are much less sensitive to the wire diameter. Since the impurities and defects can be significantly reduced during the thermal treatment, the thermally annealed Bi nanowires are purer, and consequently their electrical resistivities show a much stronger dependence on wire diameter [Fig. 2(a)]. We also note that R increases slightly with decreasing T when $T<4.0\,\mathrm{K}$ for the as-prepared samples [Fig. 3(a)], and we attribute this phenomenon to diffusive electron-electron interactions, as discussed further in terms of localization phenomena (see Sec. IV D).

Figure 3(b) shows $R(T)/R(300\text{ K})$ for a 60 nm-diameter 0.1 at. % Te-doped Bi nanowire array before and after thermal annealing. $R(T)/R(300\text{ K})$ of the as-prepared Te-doped sample [Fig. 3(b)] shows a very different behavior from that of the undoped sample with comparable wire diameter (Fig. 3(a), 65 nm), with the Te-doped sample showing a more metallic $R(T)$ behavior. Based on the theory discussed in Sec. III, the doped 60-nm Bi wire with a $[10\bar{1}1]$ orientation [in Fig. 3(b)] is still a semimetal with a much reduced band

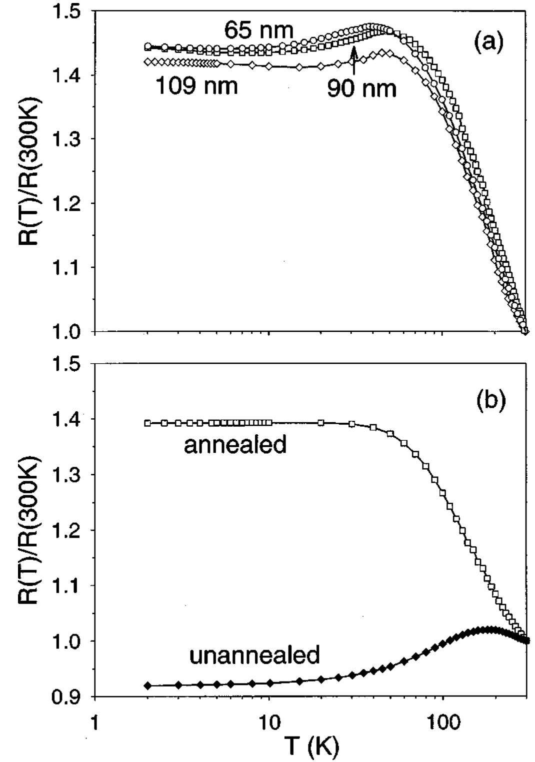

FIG. 3. (a) Resistance (normalized to the 300-K value) as a function of T (on a log scale) for as-prepared Bi nanowire arrays of various wire diameters. (b) Resistance (normalized to the 300-K value) as a function of T for a 0.1 at. % Te-doped Bi nanowire array with an average wire diameter of 60 nm before and after thermal annealing at 150 °C for 8 h under flowing N_2.

overlap between the L-point conduction band and the T-point valence band. In a metallic Bi wire, the impurity energy level of the Te dopant is in the conduction band, and every Te atom should contribute one free electron to the Bi conduction electrons. Therefore the carrier concentration is expected to show only a weak T dependence at low temperatures. Consequently, the Te-doped Bi nanowires are expected to exhibit a more metallic T dependence than their undoped counterpart. At high temperatures ($T>200\,\mathrm{K}$), the increase in carrier concentration with increasing T due to the thermal excitation of carriers from the valence band to the conduction band in the nanowires becomes dominant, and consequently, $R(T)$ decreases with further increase in T. As for the perhaps surprising result on the thermally annealed Te-doped sample, it is possible that most of the Te dopants have been segregated from the Bi lattice to the wire boundary during the annealing process (see also discussion in Sec. IV B), so that the annealed Te-doped Bi nanowires behave more like intrinsic nanowires than like heavily doped Bi nanowires [Fig. 3(b)].

B. Magnetoresistance

Since a magnetic field B can change the trajectory of the conduction electrons, it provides a convenient tool for studying the electronic transport properties of Bi nanowires. Because Bi has a large classical magnetoresistance, the effect of a magnetic field on the electrical conductivity of Bi nanowires is more complicated than in an ordinary metallic wire, and is also more interesting. The theory of low-field galvano-

magnetic effects in bulk Bi is well established.[23] In a weak magnetic field where the magnitude of each term satisfies $(\mu\cdot\mathbf{M_B})/c<1$ ($\mathbf{M_B}$ is the skew-symmetric matrix form of the vector $\mathbf{B}$), the conductivity tensor in a $\mathbf{B}$ field can be expanded in powers of $\mathbf{B}$:

$$\sigma_{ij}(\mathbf{B})=\sigma_{ij}^{0}-\sigma_{ij,k}^{1}B_k-\sigma_{ij,kl}^{2}B_kB_l+\ \ldots. \tag{8}$$

In this representation, the total conductivity is obtained by summing contributions from each carrier ellipsoid. For bulk Bi, the three electron pockets are equivalent in zero magnetic field, and after summing contributions from each ellipsoid, there are only 12 nonzero tensor components[23] for the total conductivity $\sigma(\mathbf{B})$ to order B^2. However, for Bi nanowires not oriented along the trigonal direction, the degeneracy for the three electron pockets is lifted. Since the subband edges recede from the bulk band edge by different amounts depending on the magnitude of their cyclotron effective masses m_c^*, the electron concentrations for the three electron pockets are no longer equal to each other (see Fig. 1). For the most general case, where $n_A\neq n_B\neq n_C$, a large number of the magnetoresistance tensor components would be nonvanishing.

For the specific case of interest to this study, where both $\mathbf{B}$ and $\mathbf{j}$ are parallel to the wire z axis, the magnitudes of $\mathbf{j}$ and $\mathbf{B}$ satisfy the equation

$$j=(\sigma_0-\sigma_2B^2)E, \tag{9}$$

and both σ_0 and σ_2 are functions of the mobility tensor components and carrier concentrations of each electron and hole ellipsoid. Therefore the low-field longitudinal magnetoresistance (MR) is equal to

$$\Delta R(B)/R(0)=(\sigma_2/\sigma_0)B^2. \tag{10}$$

Since bulk Bi has a very high carrier mobility at low temperatures, the parabolic dependence of $\Delta R(B)/R(0)$ on B only holds for very small B [$B\approx$ several gauss at $T=4.23$ K (Ref. 23)]. However, in Bi nanowires, the carrier mobility is much smaller than that of a perfect bulk single crystal, and therefore the condition $(\mu\cdot\mathbf{M_B})/c<1$ can be satisfied to a much higher magnetic field.

Figure 4 shows the longitudinal MR of the as-prepared Bi nanowire arrays with two different wire diameters measured at 2.0 K. For both samples, the longitudinal MR $\Delta R(B)/R(0)$ increases parabolically with B field at low fields, as expected from Eq. (10). However, the measured $\Delta R(B)/R(0)$ gradually flattens out, reaches a maximum at $B=B_m$, and finally decreases when $B>B_m$. The peak position B_m in Fig. 4 is shifted from ~3.6 T for the 65-nm sample to ~2.6 T for the 90-nm sample. The decreasing longitudinal MR at high B field can be attributed to the reduced wire boundary scattering for carriers associated with the classical size effect, as discussed below.

The classical size effect on the electrical conductivity of a thin metallic wire, with a diameter larger than the quantum confinement limit, has been well established.[1,30] In order to take wire boundary scattering into account, a parameter called the specularity coefficient ρ $(0\leqslant\rho\leqslant1)$ was introduced,[1] which gives the probability that an electron is elastically scattered at the boundary. If $\rho=1$, all boundary scattering of electrons is elastic, and the conductivity of a thin wire would be the same as that of a large specimen. For more realistic thin wire systems, ρ depends on the specific materials system, the characteristics of the wire surface, and the incident angle of the electron with respect to the boundary. Consequently, the conductivity of a thin wire is always smaller than that of the bulk material. The problem of calculating the magnetoconductivity of a thin wire with a magnetic field established along the wire axis ($\mathbf{B}\|\mathbf{I}$, where $\mathbf{I}$ denotes the current) could be solved by using kinetic theory.[2] In this case, the trajectories of the majority of electrons are helical between collisions with the boundary (except for those with $\mathbf{v}\|\mathbf{B}$, where $\mathbf{v}$ is the velocity). In the plane normal to the wire axis, the projections of the electron trajectories are a circle or a portion of a circle. Therefore the mean time between two boundary collisions for electrons increases compared to the zero-field case, and the effect of wire boundary scattering on the electrical conductivity decreases with increasing $\mathbf{B}$ field. Consequently, the electrical resistivity of a thin wire with $\mathbf{B}\|\mathbf{I}$ will be smaller than its zero-field value, giving rise to a negative magnetoresistance.

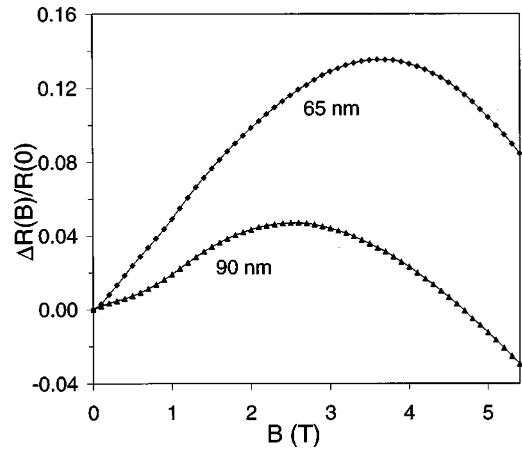

FIG. 4. Longitudinal MR $\Delta R(B)/R(0)$ as a function of B at 2.0 K for Bi nanowire arrays with average wire diameters of 65 and 90 nm before thermal annealing.

For the Bi nanowires embedded in a dielectric matrix that are examined in this work, the situation could be much more complicated than the idealized model presented in Refs. 1 and 2. The diameters of the Bi nanowires studied in this work are small ($d_w\leqslant110$ nm) and are in the quantum confinement regime. The wire boundary scattering for electrons inside a quantum wire could follow a very different scenario. For an ideal quantum wire, where the wire boundary is perfectly sharp and stoichiometrically clean, and the energy barrier at the boundary is infinitely high, the electrons should not experience any boundary scattering at low enough temperature because electrons do not have transverse momenta, and the amplitude of the electron wave function at the wire boundary is zero. In this case, the mean free path of electrons inside a quantum wire would be the same as that in a bulk specimen. However, for a real materials system, such as the Bi nanowires, the boundary conditions are far from ideal and the energy barrier at the boundary is finite. Due to the small diameter of our Bi nanowires, it is more realistic to treat the wire boundary as a finite layer of Bi atoms with a substantially higher defect concentration than in the interior of the wire. Therefore we should expect there to be a finite ampli-

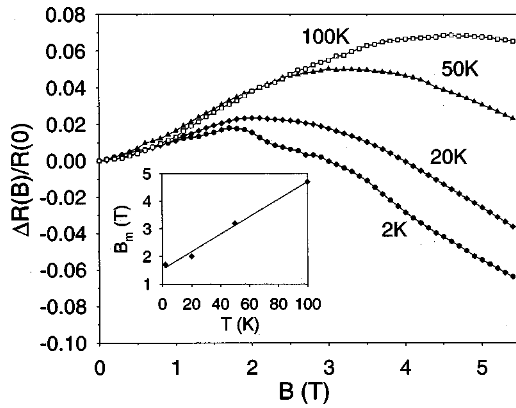

FIG. 5. Longitudinal MR $\Delta R(B)/R(0)$ as a function of B at various temperatures for a Bi nanowire array of 90-nm diameter after thermal annealing at 150 °C for 8 h under flowing N_2. The inset shows the peak position B_m as a function of T, and the solid line is the least-squares fit of the data points to a linear function.

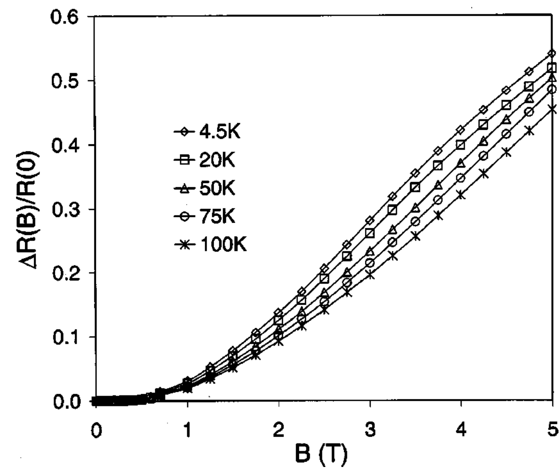

FIG. 6. Transverse MR $\Delta R(B)/R(0)$ as a function of B at various temperatures for a Bi nanowire array of 65-nm diameter before thermal annealing.

tude of the electron wave function at the wire/matrix interface, and electrons will thus experience substantial wire boundary scattering. When a magnetic field $\mathbf{B}\|\mathbf{I}$ is applied, we should also expect a reduction in the resistivity of the Bi nanowires, as is predicted by Chambers' theory.[2] Furthermore, the specularity coefficient ρ depends on the incident angle of the electron with respect to the boundary, and ρ increases when the electron trajectory becomes helical,[3] which also contributes to the reduced wire boundary scattering when a longitudinal magnetic field is applied. This is exactly what we observed in this study (Fig. 4).

We also measured the longitudinal MR at higher temperatures, and Fig. 5 shows the longitudinal MR results at four temperatures for a 90-nm Bi nanowire array after it was thermally annealed at 150 °C for 8 h under flowing N_2 (the effects of thermal annealing are discussed below), and B_m was determined at each temperature. From the inset in Fig. 5, we note that B_m (the magnetic field where the longitudinal MR is a maximum) has a roughly linear dependence on T. The theory developed by Chambers[2] can also qualitatively explain the T dependence of the peak position B_m observed here. When T increases, the volume mean free path l_0 decreases due to the stronger electron-phonon scattering, so that the wire boundary scattering becomes less important. Therefore a higher magnetic field is needed at higher T to generate the same amount of resistivity reduction associated with the reduced wire boundary scattering.

To verify our interpretation of the longitudinal MR data, we measured the transverse MR ($\mathbf{B}\perp\mathbf{I}$) for all samples at various temperatures. Figure 6 shows the transverse MR at various T for one of the samples before thermal annealing, where the transverse MR increases monotonically with magnetic field for $0 \leq B \leq 5$ T. This is as expected, since the wire boundary scattering cannot be reduced by a magnetic field perpendicular to the wire axis. We also measured the longitudinal MR of a 0.1 at. % Te-doped Bi nanowire array, and the results are shown in Fig. 7. The longitudinal MR for the Te-doped nanowire sample is very different from that of the undoped samples. Here we only observe the longitudinal MR to *increase* with magnetic field, and this result is also consistent with theory. Since the volume scattering by impurities should be the dominant scattering process in heavily Te-doped Bi nanowires, the magnetic field would only have a very small effect in changing the mean free path of the carriers in a heavily doped sample.

In Sec. IV A, we attributed the difference in the zero-field $R(T)$ between samples before and after thermal annealing to the reduced impurity concentration in the annealed samples. This argument can be tested by the longitudinal MR results. Figure 8 shows the longitudinal MR for one of the Bi nanowire arrays before and after thermal annealing. For all samples that we studied, the peak position B_m shifts to a lower field after thermal annealing. Similar to the discussion of the T dependence of B_m, the shift of B_m towards lower fields could be attributed to a longer volume mean free path l_0. The results shown in Fig. 8 indicate that Bi nanowires become purer after thermal treatment. In Fig. 8, we also observed some small oscillations in the curve of the annealed sample. This oscillatory phenomenon is discussed elsewhere.[31]

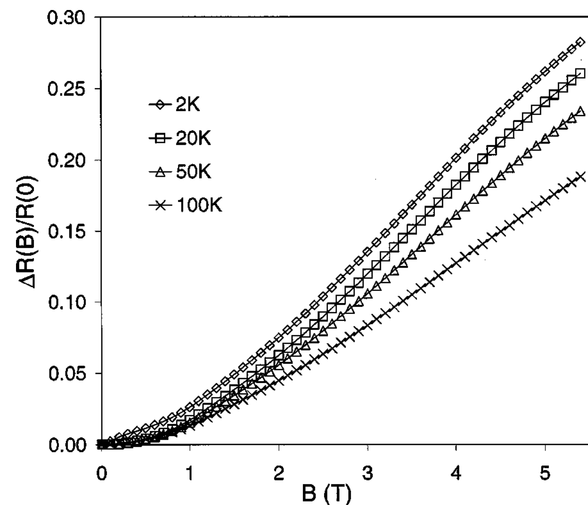

FIG. 7. Longitudinal MR $\Delta R(B)/R(0)$ as a function of B at various temperatures for a 0.1 at. % Te-doped Bi nanowire array of 60-nm diameter, after thermal annealing at 150 °C for 8 h under flowing N_2.

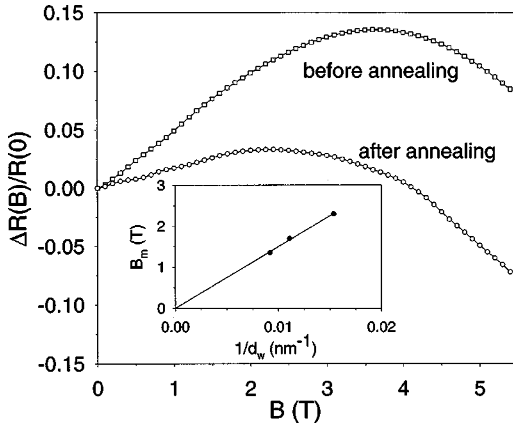

FIG. 8. Longitudinal MR $\Delta R(B)/R(0)$ as a function of B at 2.0 K for a Bi nanowire array with an average wire diameter of 65 nm before and after thermal annealing. The peak position B_m shifts to a lower field after thermal annealing, which was also observed for Bi nanowire arrays with other wire diameters. Small oscillations can be seen in the curve for the annealed sample. The inset presents the peak position B_m of the longitudinal MR determined for our nanowires as a function of $1/d_w$, the reciprocal of the wire diameter. The solid line is the least-squares fit of the data points to Eq. (11).

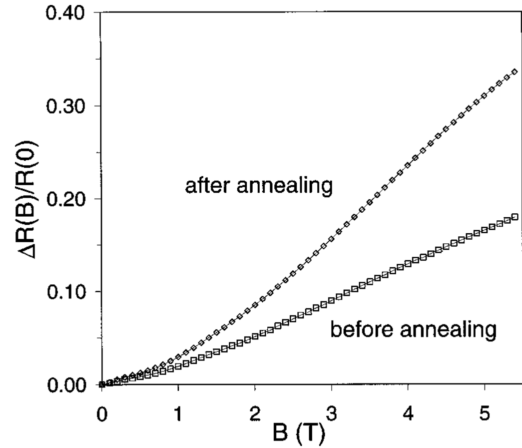

FIG. 9. Longitudinal MR $\Delta R(B)/R(0)$ at 2.0 K as a function of B for a 0.1 at. % Te-doped 60-nm Bi nanowire array before and after thermal annealing at 150 °C for 8 h under flowing N_2.

In an early study of classical size effects in single-crystal Bi microwires ($d_w \geq 250$ nm) prepared by pressure injection of Bi melt into a glass microtube,[3] it was found that the peak position B_m had a linear dependence on the reciprocal of diameter d_w,

$$B_m \approx B_{\mathrm{cut}} = \frac{D_{\mathrm{max}} c}{e d_w}, \tag{11}$$

where B_{cut} is the ''cutoff'' magnetic field for Shubnikov–de Haas oscillations,[3] D_{max} is the maximum diameter of the extremal crosssection of the Fermi surface in the plane normal to the wire axis, e is the electron charge, and c is the velocity of light. By fitting the experimental results to Eq. (11), a value $D_{\mathrm{max}} = 2.2 \times 10^{-21}$ g cm/s was obtained.[3]

In order to compare our results with those in Ref. 3, we also plotted B_m at $T = 2.0$ K as a function of $1/d_w$ for the three annealed samples with different diameters, and the result is presented in the inset of Fig. 8. We found that the three data points in the inset of Fig. 8 fit remarkably well with Eq. (11) (solid line), and D_{max} for our samples was determined to be 2.4×10^{-21} g cm/s, which also matches well with the D_{max} value obtained in Ref. [3]. Since B_m is also a function of T, for higher temperatures, $B_m(d_w)$ does not satisfy Eq. (11).

We also studied the effects of thermal annealing on the Te-doped Bi nanowire sample. Figure 9 shows the longitudinal MR at 2.0 K for the 0.1 at. % Te-doped 60-nm Bi nanowire array before and after thermal annealing. We note that the magnetoresistance increases in both cases with magnetic field. However, the thermally annealed sample showed higher MR than the as-prepared sample. This probably indicates that some of the Te dopants had been pushed out of the Bi lattice by the annealing process, so that the Te-doped Bi nanowires become more pure after thermal annealing. This interpretation is confirmed by the different T dependences of the resistance for the Te-doped Bi nanowire array before and after thermal annealing shown in Fig. 3(b).

C. Temperature dependence of the longitudinal magnetocoefficient

We also measured the T dependence of the longitudinal magnetocoefficient for Bi nanowire arrays of different wire diameters, where we focused our attention on the low B regime. At low magnetic fields $[(\mu \cdot \mathbf{M_B})/c < 1]$, the longitudinal MR satisfies the relation $\Delta R(B)/R(0) = \sigma_2 B^2/\sigma_0$ [Eq. (10)]. In these studies, R was measured at $B = 0$ and 1 T over a wide range of temperatures, and the magnetocoefficient was then calculated using $\sigma_2/\sigma_0 = [R(1\ \mathrm{T}) - R(0)]/R(0)$, which is valid as long as $R(B)$ exhibits a parabolic dependence on B up to $B = 1$ T. Figure 10(a) illustrates the experimental results for $[R(1\ \mathrm{T}) - R(0)]/R(0)$ for Bi nanowire arrays of three different wire diameters before thermal annealing. We note that the magnetocoefficient decreases monotonically with increasing T for the 65-nm Bi nanowire array, while for the 90- and 109-nm samples, the T dependence of the magnetocoefficient is more complicated. At very low temperatures ($T < 10$ K), the magnetocoefficient increases sharply with decreasing T for the 90- and 109-nm samples, which can be attributed to localization effects (to be addressed further in Sec. IV D). For $T > 10$ K, the magnetocoefficient for these two samples first increases with increasing T until $[R(1\ \mathrm{T}) - R(0)]/R(0)$ reaches its peak value at T_m, beyond which $[R(1\ \mathrm{T}) - R(0)]/R(0)$ decreases with further increase in T. The annealed samples also show a similar trend, and the results for the annealed samples are illustrated in Fig. 10(b), where $[R(1\ \mathrm{T}) - R(0)]/R(0)$ is shown to be essentially independent of wire diameter at high temperatures ($T > 100$ K).

In Ref. 14, we proposed a possible explanation for this phenomenon based on the assumption of quantized transverse momenta of the carriers. Based on the electronic band structures shown in Fig. 1, the increasing magnetocoefficient with increasing T in the regime $T < T_m$ for the unannealed 90- and 109-nm samples was attributed to an increase of the ratio of the electron concentration in electron pocket A to that in pockets B and C with increasing T. Such a mechanism

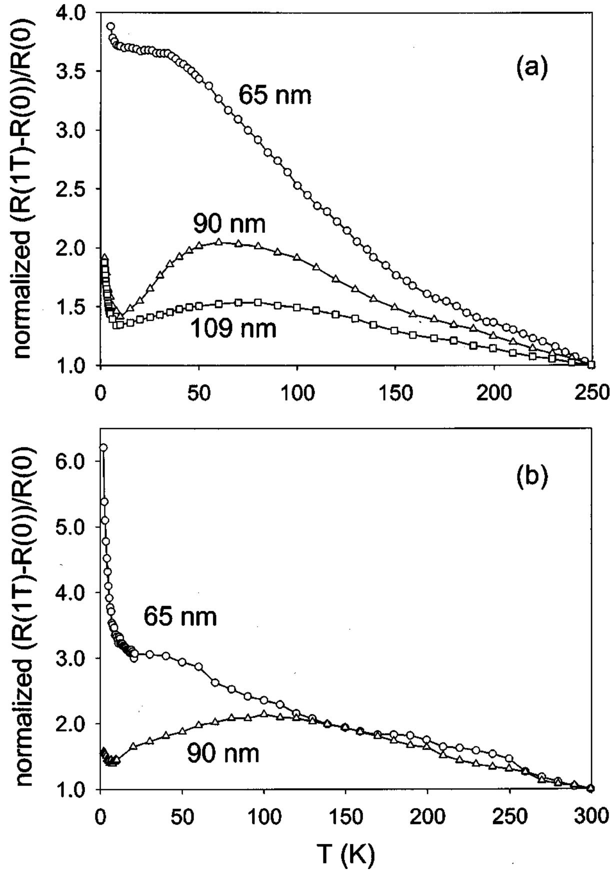

FIG. 10. (a) Temperature dependence of the longitudinal magnetocoefficient $\sigma_2/\sigma_0 = [R(1\,\mathrm{T})-R(0)]/R(0)$ for as-prepared Bi nanowire arrays of various wire diameters. The data are normalized to the magnetocoefficient at 250 K. (b) The normalized longitudinal magnetocoefficient as a function of T for Bi nanowire arrays after thermal annealing at 150 °C for 8 h. The data are normalized to the magnetocoefficient at 300 K.

was found to be unimportant for the 65-nm sample because the electron concentration in pocket A is negligible for the 65-nm Bi nanowire at $T \leqslant 100\,\mathrm{K}$.[31] Although the magnetocoefficient σ_2/σ_0 for electrons in pocket A is about three times larger than that in pockets B and C, more detailed theoretical calculations indicate that such a mechanism cannot by itself explain the experimental results.

Another mechanism that may also contribute to the experimental results shown in Figs. 10(a) and (b) is the wire boundary scattering for carriers. As discussed in Sec. IV B (see insets in Figs. 5 and 8), the importance of wire boundary scattering for carriers strongly depends on both the wire diameter and the temperature. Since the peak position of the longitudinal magnetoresistance B_m shifts to higher fields when T increases (inset in Fig. 5), the magnitude of the reduction in wire boundary scattering by a magnetic field of $B=1$ T also decreases with increasing T, and this effect may result in a larger $R(1\,\mathrm{T})$ at higher temperatures in the 90- and 109-nm Bi nanowire samples. Consequently, $[R(1\,\mathrm{T})-R(0)]/R(0)$ increases with increasing T in the temperature range $T<T_m$ for those two samples. However, for the 65-nm sample, B_m has shifted to magnetic fields much higher than 1 T at all temperatures investigated (see Fig. 8). Therefore the reduction in wire boundary scattering at $B=1$ T is less important and is also less sensitive to T for the 65-nm sample; consequently, its magnetocoefficient decreases monotonically with increasing T due to the stronger phonon scattering at higher temperatures.

D. Electrical resistance of Bi nanowires at very low temperatures

For a disordered system at very low temperatures (typically $T \leqslant 5.0\,\mathrm{K}$), the electron conduction becomes diffusive, and localization effects and diffusive electron-electron interactions become important. Localization effects in disordered systems have been extensively studied both theoretically and experimentally.[4] They refer to quantum interference effects, which are usually observed only at low temperatures in low mobility samples where the electron phase-coherence length is much larger than its mean free path. For a wire with a small diameter, when both the electron phase-breaking length L_ϕ and the magnetic length L_B are larger than the wire diameter d_w, the localization behavior should be regarded as one dimensional. Theory predicts[5,32,33] that the contribution from 1D localization to the electrical resistance is given by

$$\Delta R(T,B)/R_0 = e^2\rho_e/(2\pi\hbar S)\{\tfrac{3}{2}[L_\phi^{-2}+\tfrac{4}{3}L_{s.o.}^{-2}+L_B^{-2}]^{-1/2} - \tfrac{1}{2}[L_\phi^{-2}+L_B^{-2}]^{-1/2}\}, \quad (12)$$

whereby the magnetic field is perpendicular to the wire axis, S is the cross-sectional area of the wire, ρ_e is the impurity resistivity, $L_{\mathrm{s.o.}}$ is the spin-orbit interaction length, and the magnetic length L_B is given by[33]

$$L_B = \left[\frac{3\hbar^2}{e^2 S B^2}\right]^{1/2}. \quad (13)$$

In the limit of $B \to 0$ and strong spin-orbit interaction, Eq. (12) is reduced to

$$\left[\frac{\Delta R}{R_0}\right]_{\mathrm{s.o.}} = -\frac{e^2\rho_e}{4\pi\hbar S}L_\phi. \quad (14)$$

Since L_ϕ increases with decreasing T,[34] we note that the spin-orbit scattering results in a decrease in the total resistance with decreasing T, producing a so-called antilocalization effect,[5] which is of the opposite sign as the usual localization effects.

For Bi at very low temperatures, the electron-electron interaction is also very strong. In one dimension, the electron-electron interaction also contributes to localization effects through a contribution to the resistance given by[35]

$$\left[\frac{\Delta R}{R_0}\right]_{e\text{-}e} = \frac{e^2\rho_e}{2^{3/2}\pi\hbar S}\left(4-\frac{3}{2}F\right)\left[\frac{D\hbar}{k_B T}\right]^{1/2}, \quad (15)$$

where F is a screening factor, and D is the electron diffusion constant. We note that the contribution to $\Delta R/R_0$ from 1D electron-electron interactions results in an increase in the resistance with decreasing T. In Bi nanowires, the T dependence of the zero-field resistance at very low temperatures will be determined by the sum of Eq. (14) and Eq. (15), and $\Delta R/R_0$ can be either positive or negative, depending upon

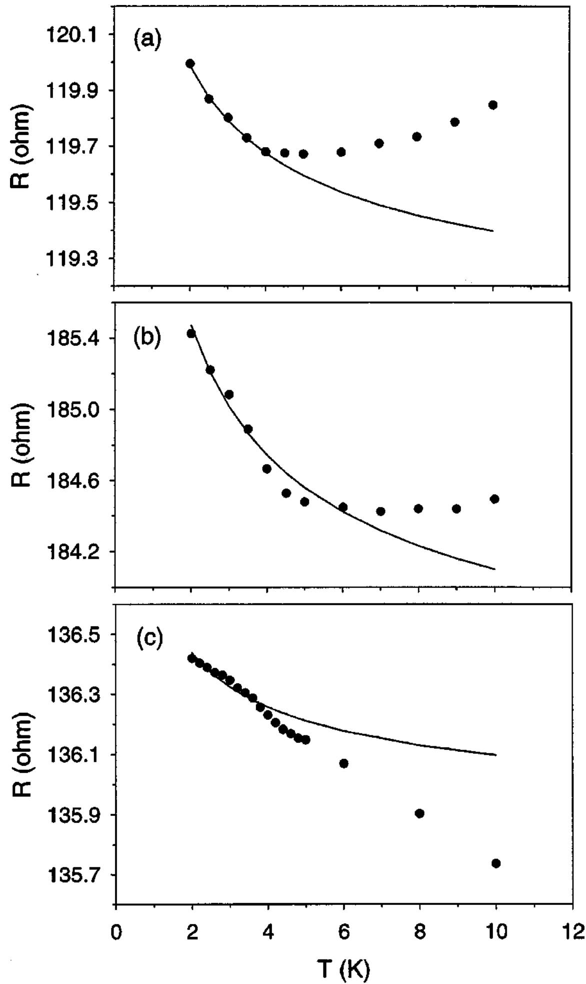

FIG. 11. Low-temperature resistance of as-prepared Bi nanowire arrays of different wire diameters as a function of T: (a) 65 nm, (b) 90 nm, and (c) 109 nm. The lines are the least-squares fits of the data points to the function of $R_0+R_1T^{-1/2}$.

the relative magnitude of these terms. These phenomena have been demonstrated in early studies of polycrystalline Bi nanowires[5] and in our studies of Bi nanowire arrays prepared by a gas phase vapor deposition process.[6]

Figure 11 shows the temperature-dependent resistance of as-prepared Bi nanowire arrays of different wire diameters at low temperatures, extracted from the data presented in Fig. 3(a). At very low temperatures ($T\leqslant 4.0$ K), the resistance of all three samples increases with decreasing T, suggesting that the electron conduction becomes diffusive and that electron-electron interactions are more important than localization effects. In Fig. 11, the solid lines are the least-squares fits of the data points at very low temperatures ($T\leqslant 4.0$ K for the 65- and 90-nm samples, and $T\leqslant 3.0$ K for the 109-nm sample) to the function of $R=R_0+R_1T^{-1/2}$. For all three samples, the data points at very low T fit well to the function $R=R_0+R_1T^{-1/2}$, in agreement with the theory of 1D electron-electron interactions [Eq. (15)].[35]

Since electron-electron interactions are not sensitive to the magnetic field, we also studied the transverse MR of Bi nanowires at very low temperatures in order to separate the contributions from localization effects and from electron-electron interactions. Since a magnetic field perpendicular to the electric current can destroy localization effects, from Eq. (14), a positive MR is expected to be observed in this case for Bi nanowires. Figure 12 shows the transverse magnetoresistance at different magnetic fields for a Bi nanowire array with an average wire diameter of 109 nm, measured 14 months after the sample fabrication. This was the only sample among the three samples of different wire diameters in Fig. 11 for which the transverse MR showed clear evidence for localization effects. From Fig. 12, we note that for $B\leqslant 0.3$ T, the transverse MR increases with decreasing T, consistent theory [Eq. (14)] which predicts that localization effects become stronger at lower temperatures.[34] At $B\geqslant 0.3$ T, the plots for $\Delta R(0.3\ \mathrm{T}/R(0)$, for $\Delta R(0.4\ \mathrm{T})/R(0)$ and for $\Delta R(0.5\ \mathrm{T})/R(0)$ as a function of temperature are almost parallel to each other, indicating that the further increase in MR (which can be attributed to the classical MR) is not sensitive to T and the contribution from localization effects saturates at $B=0.3$ T. The observation of a strong classical MR in the temperature range of $2.0\leqslant T \leqslant 4.0$ K indicates that in our experiments we have not yet reached a low enough temperature range where localization effects become dominant.

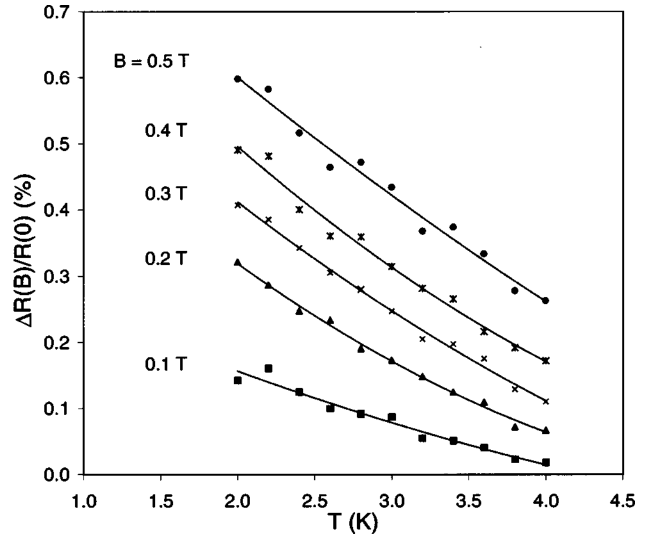

FIG. 12. transverse MR $\Delta R(B)/R(0)$ of a Bi nanowire array with an average wire diameter of 109 nm as a function of T at different magnetic fields measured 14 months after the sample fabrications. The solid lines are guides to the eye.

The experimental results that we obtained in this study are consistent with earlier studies on localization effects in polycrystalline Bi nanowires.[5] In Ref. 5, the transverse MR was always found to be positive, and it disappeared when $T \geqslant 3.0$ K, which was attributed to vanishing localization effects at $T\geqslant 3.0$ K, and a very small classical MR was observed in their polycrystalline Bi nanowires. Localization effects were found to be dominant only in the range $T\leqslant 1.0$ K. Localization effects in our single-crystal Bi nanowire arrays have only been observed at very low temperatures ($T\leqslant 4.0$ K), because at high temperatures, the inelastic scattering for electrons introduces random fluctuations in the time evolution of an electronic state, which limits the quantum interference necessary for the observation of localization effects.[4,36] We thus conclude that the diffusive electron conduction is not an important issue for our Bi nanowires at $T \geqslant 4.0$ K and that localization effects do not become dominant

even at T as low as 2.0 K. The study of localization phenomena confirms that the semiclassical transport model used in this paper is applicable to the transport properties of Bi nanowires for $T \geqslant 2.0$ K, and that our discussion of the quantum confinement and classical magnetoresistance effects is valid for this temperature regime ($T \geqslant 2.0$ K).

V. SUMMARY

We have studied the electronic transport properties of ultrafine single-crystal Bi nanowire arrays with various wire diameters over a wide range of temperatures and magnetic fields. Most experimental results are in good agreement with theory, and can be explained by an electronic subband structure of quasi-1D Bi nanowires based on the electronic structure of 3D bismuth and the theory of wire boundary scattering for carriers. The quantum confinement of carriers plays an important role in determining the overall temperature dependence of the zero-field resistivity of Bi nanowires. Although we observed evidence for a localization effect at low temperatures ($T < 4.0$ K), localization effects are not the dominant mechanism affecting either the resistivity or the magnetoresistance in the temperature range of this study ($2.0\ \mathrm{K} \leqslant T \leqslant 300$ K). Unlike bulk Bi or polycrystalline Bi nanowires, where the electron-electron interaction is the dominant scattering process for carriers at low temperatures, we found that the wire boundary scattering for carriers is very important for single-crystal Bi nanowires of small diameter.

ACKNOWLEDGMENTS

We thank Dr. G. Dresselhaus of MIT and Professor G. Chen of UCLA for valuable discussions. This project is partially funded by the U.S. Navy (Contract No. N00167-98-K0024), the National Science Foundation (Grant No. DMR-98-04734), and the ONR/MURI Program (Subcontract No. 0205-6-G-7A114-01).

*Present address: Lucent Technologies Bell Labs, 9333 S. John Young Parkway, Orlando, FL 32819.

†Present address: Lucent Technologies Bell Labs, 1 Robbins Rd., Westford, MA 01886.

‡Author to whom correspondence should be addressed.

[1] R. B. Dingle, Proc. R. Soc. London, Ser. A **201**, 545 (1950).

[2] R. G. Chambers, Proc. R. Soc. London, Ser. A **202**, 378 (1950).

[3] N. B. Brandt, D. V. Gitsu, A. A. Nikolaeva, and Y. G. Ponomarev, Zh. Éksp. Teor. Fiz. **72**, 2332 (1977) [Sov. Phys. JETP **45**, 1226 (1977)].

[4] P. A. Lee and T. V. Ramakrishnan, Rev. Mod. Phys. **57**, 287 (1985).

[5] D. E. Beutler and N. Giordano, Phys. Rev. B **38**, 8 (1988).

[6] J. Heremans, C. M. Thrush, Z. Zhang, X. Sun, M. S. Dresselhaus, J. Y. Ying, and D. T. Morelli, Phys. Rev. B **58**, R10 091 (1998).

[7] B. J. van Wees, H. van Houten, C. W. J. Beenakker, J. G. Williamson, L. P. Kouwenhoven, D. van der Marel, and C. T. Foxon, Phys. Rev. Lett. **60**, 848 (1988).

[8] C. J. Muller, J. M. van Ruitenbeek, and L. J. de Jongh, Phys. Rev. Lett. **69**, 140 (1992).

[9] L. Olesen, E. Laegsgaard, I. Stensgaard, F. Besenbacher, J. Schiotz, P. Stoltze, K. W. Jacobsen, and J. K. Norskov, Phys. Rev. Lett. **72**, 2251 (1994).

[10] R. Landauer, IBM J. Res. Dev. **1**, 223 (1957).

[11] Z. B. Zhang, J. Y. Ying, and M. S. Dresselhaus, J. Mater. Res. **13**, 1745 (1998).

[12] L. D. Hicks and M. S. Dresselhaus, Phys. Rev. B **47**, 12 727 (1993).

[13] J. Heremans and C. M. Thrush, Phys. Rev. B **59**, 12 579 (1999).

[14] Z. B. Zhang, X. Z. Sun, M. S. Dresselhaus, J. Y. Ying, and J. P. Heremans, Appl. Phys. Lett. **73**, 1589 (1998).

[15] Z. B. Zhang, D. Gekhtman, M. S. Dresselhaus, and J. Y. Ying, Chem. Mater. **11**, 1659 (1999).

[16] D. Schiferl and C. S. Barrett, J. Appl. Crystallogr. **2**, 30 (1969).

[17] R. T. Isaacson and G. A. Williams, Phys. Rev. **185**, 682 (1969).

[18] V. S. Edel'man, Adv. Phys. **25**, 555 (1976). Equation for the Lax model in this paper is in error by a factor of 2.

[19] G. E. Smith, G. A. Baraff, and J. M. Rowell, Phys. Rev. **135**, A1118 (1964).

[20] B. Lax and J. G. Mavroides, in *Advances in Solid State Physics* (Academic Press, New York, 1960), Vol. 11.

[21] M. S. Dresselhaus and M. P. Vecchi (unpublished).

[22] M. P. Vecchi and M. S. Dresselhaus, Phys. Rev. B **10**, 771 (1974).

[23] R. Hartmann, Phys. Rev. **181**, 1070 (1969).

[24] J. P. Michenaud and J. P. Issi, J. Phys. C **5**, 3061 (1972).

[25] R. J. Dinger and A. W. Lawson, Phys. Rev. B **7**, 5215 (1972).

[26] N. B. Brandt, V. V. Moshchalkov, and S. M. Chudinov, Zh. Éksp. Teor. Fiz. **74**, 1829 (1978) [Sov. Phys. JETP **47**, 953 (1978)].

[27] M. Gurvitch, J. Low Temp. Phys. **38**, 777 (1980).

[28] P. Fischer, I. Sosnowska, and M. Szymanski, J. Phys. C **11**, 1043 (1978).

[29] K. K. Gopinathan and A. R. K. L. Padmini, Solid State Commun. **16**, 817 (1975).

[30] E. R. Andrew, Proc. Phys. Soc. London, Sect. B **62**, 77 (1949).

[31] Z. B. Zhang, Ph.D. thesis, Massachusetts Institute of Technology, 1999.

[32] P. Santhanam, S. Wind, and D. E. Prober, Phys. Rev. Lett. **53**, 1179 (1984).

[33] B. L. Al'tshuler and A. G. Aronov, Pis'ma Zh. Éksp. Teor. Fiz. **33**, 515 (1981) [JETP Lett. **33**, 499 (1981)].

[34] B. L. Al'tshuler, A. G. Aronov, and D. E. Khmel'nitzkii, J. Phys. C **15**, 7367 (1982).

[35] B. L. Al'tshuler, A. G. Aronov, and P. A. Lee, Phys. Rev. Lett. **44**, 1288 (1980).

[36] D. J. Thouless, Phys. Rev. Lett. **39**, 1167 (1977).